THE ASTROPHYSICAL JOURNAL, 531:591–598, 2000 March 1
Copyright is not claimed for this Article. Printed in U.S.A.

LINEAR r-MODES BELOW THE SUN'S CONVECTIVE ENVELOPE

CHARLES L. WOLFF
NASA Goddard Space Flight Center, Greenbelt, MD 20771; charles.wolff@gsfc.nasa.gov
Received 1999 May 11; accepted 1999 October 18

ABSTRACT

Theoretical properties of linear r-modes in a standard solar interior are computed, and the excitation of some by convective overshoot is estimated. The modes oscillate in a resonant cavity usually occupying most of the nonconvecting interior. Most modes concentrate their kinetic energy toward the center of the Sun. Over half the energy usually lies below 0.15 $R_\odot$ with an asymptotic limit of 0.11 $R_\odot$ for high radial harmonics ($R_\odot$ is the solar radius). The oscillation frequencies are very close to the well-known toroidal frequency, $\sigma_t = 2\Omega m[l(l+1)]^{-1}$, deviating by fractional amounts $\sim 10^{-6\pm1}$ which are roughly 3 orders of magnitude smaller than deviations found earlier for r-modes in convective layers. An explicit formula for the ratio of divergent motion to curl motion is derived. It shows how rapidly the compressible component changes as a function of r. Compressibility is only $\sim 10^{-6}$ of the total motion for low l-modes and declines proportionally to ml^{-3} for high l. A small subset of modes (the lowest radial harmonic of angular states $|m| = l$) avoid the core which makes them sensitive to convective overshoot. Just one of the giant convection cells detected by Beck et al. can excite such modes to kilometer-size amplitudes with the possibility that far larger displacement amplitudes can accumulate in the mode over time if the interaction between cells and r-modes is found to be strong.

Subject headings: convection — hydrodynamics — stars: oscillations — Sun: interior — Sun: oscillations

1. INTRODUCTION

The r-modes are small-amplitude oscillations of a nearly spherical, rotating star in which the Coriolis force dominates the oscillation. The motion is almost entirely perpendicular to the local gravity vector in nonconvecting layers. There are two branches of solutions, which Wolff (1998) called "slow" and "fast" based on their respective rotation rates in inertial space. The fast modes reduce to steady geostrophic flow in a stellar fluid which is otherwise rotating as a solid body. The slow modes are the subject of this paper and have nonzero oscillation frequencies relative to the fluid. Rossby waves of Earth meteorology (Longuet-Higgins 1964) are a special case of the slow r-modes applied to a thin shell in which the curvature of the sphere is often negligible. In astronomy, most work is for stars rotating slowly and uniformly. Provost, Berthomieu, & Rocca (1981; hereafter PBR) and Smeyers, Craeynest, & Martens (1981) derived the basic equation. If differential rotation is significant, the approach of Papaloizou & Pringle (1978) may be useful or the perturbation method of Wolff (1998) who showed that rotational shear can destroy some r-modes when it is as strong as it is in the outer 20% of the Sun's radius. Since shear in the deep solar interior is thought to be a factor of 10 less and is not even measured in the core region, differential rotation will be ignored in this paper, which concerns the Sun below its convective envelope.

If r-modes are excited, either the Sun's convective envelope or its radiative interior can act as a resonant cavity that traps the modes. Wolff & Blizard (1986, hereafter WB) studied those trapped in the envelope and showed that the cavity has rather sharp boundaries near the solar surface and at the base of the convective zone. A third sharp boundary lies close to the Sun's center in a standard solar model where a term often seen in spherical problems, $l(l+1)r^{-2}$, becomes dominant and reflects oscillation energy back into the cavity.

One goal of this paper is to add more quantitative detail to the behavior of r-modes in the Sun. It is valuable to see where the energy is concentrated and to what degree as a function of radial distance. It is also important to know where the vorticity dominated motion has a non negligible compressive component. Another goal is to begin studies of possible excitation mechanisms. An analytic expression is given for momentum transfer to oscillation modes from a general force. Then the force is specified by a simple model of convective overshoot to estimate how much it will excite the modes. If r-modes are active in the radiative interior, their low radial harmonics will probably affect the giant cells of the convection zone (Beck, Duvall, & Scherrer 1998) and thereby create—or at least redistribute—some of the Sun's surface features.

In § 2, some known basic properties are summarized. In § 3, simple results are discussed under the approximation that the r-mode displacement amplitude varies rapidly with radial distance compared to the solar interior structure (WKB approximation). In § 4, the results of exact integrations are presented to show the oscillation frequencies, radial dependence of the modes, and the relative sizes of the compressible and incompressible components of the motion. In § 5, the effect of one possible excitation mechanism (convective overshoot) is explored.

2. KNOWN PROPERTIES OF LINEAR r-MODES

2.1. *Main Parameters*

An r-mode has a motion which is primarily horizontal and incompressible in stably stratified layers. This is also true in convecting layers except where the superadiabatic gradient is extremely small (see also last remark in this section). Excepting very high radial harmonics, the oscillation frequency usually differs little from the value

$$\sigma_t = \frac{2\Omega m}{l(l+1)} \tag{1}$$

given by Papaloizou & Pringle (1978) for a star rotating slowly at a constant rate Ω. The oscillation frequency is with respect to coordinates rotating with the star. Integers l and m are the angular harmonic numbers.

From the general equations (e.g., Cox 1980; Unno et al. 1989) for linear, adiabatic oscillations of a star, PBR and Smeyers et al. (1981) derived what is called herein the "r-mode equation," the most compact form of which is given in § 2.3. The equation is valid for nearly spherical stars rotating uniformly. More precisely, a rotation parameter,

$$\varepsilon = \frac{\Omega}{\Omega_g}, \tag{2}$$

must be small compared to unity, where $\Omega_g = (GMR^{-3})^{0.5}$, G is the gravitational constant, M is the mass, and R the radius of the star. For a rotation rate $\Omega = 2\pi$ (400 nHz) of the deep solar interior, one finds $\varepsilon = 0.00401$. Terms of higher order than ε^2 are ignored herein. The oscillation frequency is

$$\sigma = \sigma_t(1 + \varepsilon^2 s + \cdots), \tag{3}$$

where Papaloizou & Pringle (1978) and Smeyers (1980) proved that the first power of ε does not enter. Numerical integration of the r-mode equation determines s and the main component of the radial eigenfunction. As PBR and WB showed, s becomes more negative as the radial harmonic number increases for all r-modes trapped below the Sun's convective envelope and the opposite is true for modes trapped in the envelope. Let $\boldsymbol{\xi}(r)e^{i\sigma t}$ be the displacement of the fluid caused by the r-mode. Using the general decomposition of a vector field and applying it to a rotating sphere, Smeyers (1980) expanded ξ into spherical harmonics $Y = Y_l^m(\vartheta, \varphi)$. Each order in ε is the same as in the nonrotating case and can be written (Aizenman & Smeyers 1977; Chandrasekhar 1961, Appendix III),

$$\boldsymbol{\xi} = \sum_{l',m'} (f_1 \hat{\boldsymbol{r}} Y + f_2 r \nabla Y - f_3 \boldsymbol{r} \times \nabla Y)_{l',m'}, \tag{4a}$$

where each f is a function of radial distance only and the three r-symbols are, respectively, a unit vector, a scalar, and a vector. In pure toroidal motion all f_1 and f_2 terms are zero; in pure spheroidal motion all f_3 terms are zero. An r-mode contains both types but, typically, just one toroidal term for one specific pair (l, m) dominates the sum so that

$$(f_1 \text{ and } f_2)_{l',m'} \sim \varepsilon^2 (f_3)_{l,m} \text{ or less}. \tag{4b}$$

This is true (Saio 1982) whenever $(\sigma - \sigma_t) \sim \varepsilon^2\Omega$ or less, which holds very well for the r-modes to be computed herein. Sometimes perfectly adiabatic stratification is assumed. This makes pure toroidal motion impossible (PBR) and results in a mixture (WB) of f_1, f_2, and f_3 components, which are called inertial modes. But Lockitch & Friedman (1999) note an exception for the lowest radial harmonic of states, $|m| = l$.

2.2. *Rotational Distortion*

The slightly ellipsoidal shape of the Sun cannot be ignored when solving the r-mode equation. Chandrasekhar (1933) found that the shape solves

$$\frac{\partial}{\partial r}\left(\frac{r^2}{\rho}\frac{\partial p}{\partial r}\right) + \frac{\partial}{\partial \mu}\left(\frac{1-\mu^2}{\rho}\frac{\partial p}{\partial \mu}\right) = r^2(2\Omega^2 - 4\pi G\rho), \tag{5}$$

where $(r, \mu = \cos\vartheta, \varphi)$ are spherical coordinates. He showed that the pressure p and density ρ are constant on the same level surface and that the surface departs from a sphere by an amount that can be described by one Legendre polynomial P_2 as long as terms smaller than $\sim\varepsilon^2$ are neglected. With equal validity, PBR defined the surface with the parameter

$$x \equiv \frac{r}{R}(1 - \varepsilon^2\alpha\mu^2)^{-1} \simeq \frac{r}{R}(1 + \varepsilon^2\alpha\mu^2 + \cdots), \tag{6}$$

where x is constant on a level surface. The complete method (Chandrasekhar-Milne) of finding $\alpha(x)$ is described by Tassoul (1978). A quick way to see its distribution is to integrate the following equation:

$$\alpha'' + \frac{2\alpha'}{H_m} + \left(\frac{1}{H_m} - \frac{3}{x}\right)\frac{2\alpha}{x} = 0, \tag{7}$$

where primes represent d/dx and $H_M = M(x)[dM(x)/dx]^{-1}$ is the scale height of mass within x. The resulting curve is shown on Figure 1 based on $M(x)$ from the model of Guenther et al. (1992). The central boundary conditions are $\alpha =$ constant and $\alpha' = 27.6\alpha x$, which come from a power series expansion about the origin. I derived equation (7) from equation (5) by changing the variable r to x using equation (6). Terms with the same angular factor must sum to zero. The μ^2 terms reduce to equation (7) after substituting an identity obtained from the dominant μ^0 terms.

Since equation (7) is homogeneous, α times a constant is also a solution. To fix the scale, one could make $\alpha(x = 1)$ consistent with the measured oblateness of the Sun. In this paper, the scale was set so that the apparent equatorial and polar diameters differ by 15.7 milliarcseconds, which is the known theoretical result for a Sun rotating uniformly at its mean surface rate. Figure 1 can be used, unchanged, for any other slow uniform rotation rate, since the value of ε contains the complete adjustment needed in equation (6) for a different rate. Notice that α never reaches zero because the level surfaces are ellipsoids all the way to the center of the star. The main reason for this is that the force (centrifugal) pushing toward an ellipsoid and the force (gravity) pushing toward a sphere are both proportional to x as x approaches zero. Thus, their ratio approaches a nonzero constant at the origin.

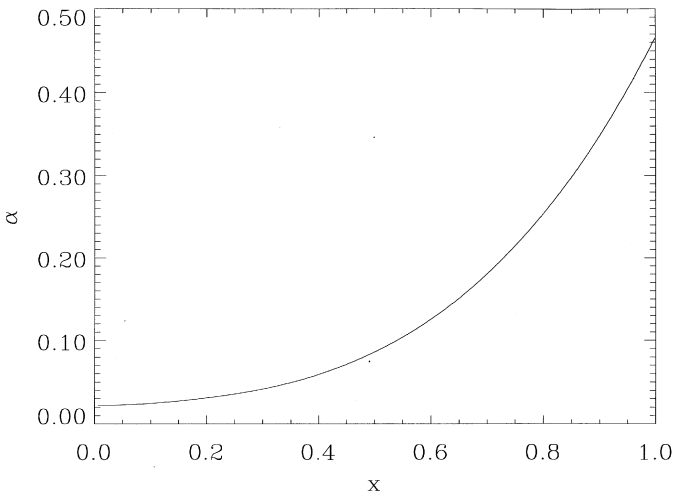


FIG. 1.—Relative amount of ellipsoidal distortion in a slowly and uniformly rotating Sun. The abscissa x is the fractional radius, and $\varepsilon^2\alpha$ controls the oblateness in eq. (6).

2.3. *The r-Mode Equation*

PBR derived the r-mode equation in dimensionless units which will be used here and in § 3 and 4 for consistency. In particular, all frequencies will be measured in units of Ω_g. The r-mode equation was reduced by WB to its shortest form, a Helmholtz equation:

$$U'' + G(x)U = 0 \,. \tag{8}$$

The sign of G determines where the radial dependence of the r-mode has sinusoidal character and where it is exponentially damped, thus defining a resonant cavity. Here

$$G = -\frac{\lambda_1 \lambda_b}{x^2}(s - \sigma_r) \,, \tag{9}$$

and

$$\lambda_b = \frac{p'}{\rho}\left(\frac{p'}{\gamma p} - \frac{\rho'}{\rho}\right) \tag{10}$$

is the square of the buoyancy frequency (Brunt-Väisälä). Table 1 gives values of λ_1 for all modes with $l \leq 6$. Figure 2 shows σ_r for two cases: $(l, m) = (2, 1)$ and $(2, 2)$. Horizontal lines are drawn at the eigenvalues, s, of the six lowest radial harmonic r-modes (as computed in § 4). Each line extends across the cavity applying to that mode. The cavity is where

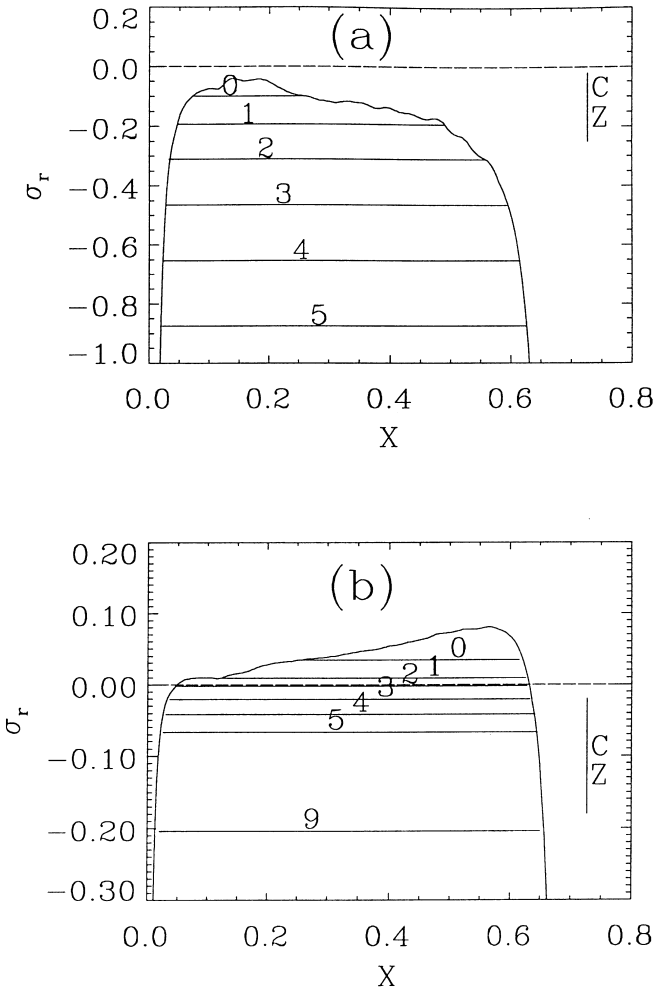


FIG. 2.—Dimensionless turning-point frequency, σ_r, for r-modes trapped below the convection zone (CZ). Plots (*a*) and (*b*) are for angular harmonics, $(l, m) = (2, 1)$ and $(2, 2)$, respectively. Horizontal lines are labeled by radial harmonic number and drawn at the eigenvalue s of each mode. Each line extends across the resonant cavity sensed by that r-mode.

TABLE 1

THE CONSTANT λ_1 FOR LINEAR r-MODES

l	$\lvert m\rvert$	λ_1
1.....	1	10.0000
2.....	1	2.7194
2.....	2	23.6250
3.....	1	5.5527
3.....	2	8.3077
3.....	3	48.0000
4.....	1	9.4845
4.....	2	11.5373
4.....	3	18.0476
4.....	4	85.9375
5.....	1	14.4492
5.....	2	16.2741
5.....	3	20.6131
5.....	4	32.8898
5.....	5	140.4000
6.....	1	20.4285
6.....	2	22.1459
6.....	3	25.7543
6.....	4	33.3653
6.....	5	53.8117
6.....	6	214.3750

$(s - \sigma_r) < 0$, since the other factors in equation (9) are positive in a nonconvecting zone. Curves of σ_r look similar for other values of l and m because they always contain two fundamental infinities—one near the origin driven by the term $-l(l+1)x^{-2} \to -\infty$ and one near the base of the convection zone where $\lambda_b'/\lambda_b \to -\infty$.

3. ASYMPTOTIC PROPERTIES

For general insight before making exact calculations, let us look at several simpler results valid under two conditions: $|s| \gg |\sigma_r|$ and the WKB approximation, $|H_p$ and $H_\rho| \gg |H_\xi|$, which relates the local scale heights of p, ρ, and ξ. The two conditions overlap to a large extent. Both hold for most r-modes except the lowest radial harmonics. However, the first condition fails near the cavity boundaries.

With the above approximations, $G \simeq (-s\lambda_1)\lambda_b x^{-2}$ and the cavity solution which WB derived for equation (8) has the oscillatory factor $\exp[\pm i\pi(\chi + \beta)]$, the real part of which locates the radial location of each node (where toroidal motion vanishes). The constant $\beta(\simeq -\frac{1}{2})$ roughly accounts for conditions below the cavity,

$$\chi = \frac{\sqrt{-s\lambda_1}}{\pi}\int_{x_0}^{x} dx \sqrt{\frac{\lambda_b}{x^2}} \,, \tag{11}$$

and x_0 is the lower boundary of the cavity. Figure 3 shows χ over its full range ($x_0 = 0$) within the nonconvecting layers. I set $-s\lambda_1 = 1$ for this graph, since $s\lambda_1$ is a constant for a given mode. Because the ordinate is proportional to "phase," the nodes and antinodes of r-modes are distributed at equal distances along that axis, ignoring the portion of the curve ($x < x_0$) which is outside the cavity. For high radial harmonics, x_0 approaches zero which implies that their nodes and antinodes will concentrate quite close to the center of the Sun. Central concentration is also strong for the low angular harmonics, $l \leq 3$, even those with a rather small radial harmonic number (see next paragraph).

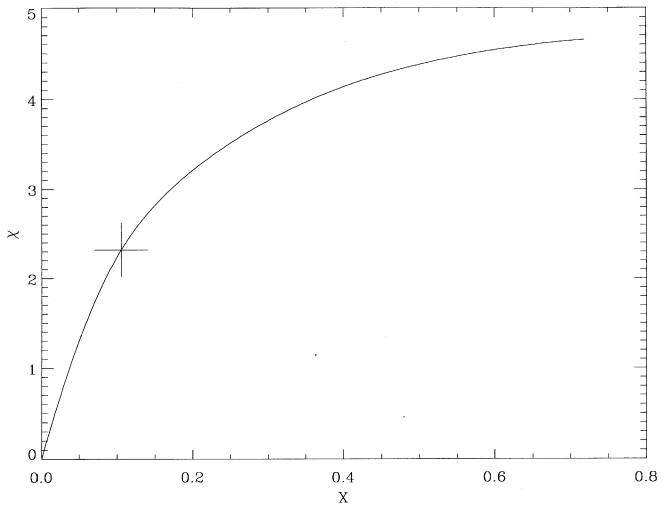


FIG. 3.—Phase function χ for $-s\lambda_1 = 1$. This estimates the radial distribution of energy, nodes, and antinodes for r-modes. Nodes are distributed almost uniformly along the ordinate, and thus concentrate toward the solar center. The curve is also the cumulative amount of energy within x for high radial harmonics. About half of their kinetic energy lies on the inner 11% of the solar radius (*plus sign*).

Figure 3 can also serve as an approximate graph of the radial distribution of kinetic energy in r-mode motion except for the lowest radial harmonics. Almost equal amounts of energy lie between any two neighboring nodes except those near a cavity boundary. This follows from a general study (Wolff 1993) of equidistribution of energy in oscillating systems. From Table 1 of that study ("V_c component" with $\varepsilon_1 = 0$) one sees that the actual quantity which is about the same when integrated between any two neighboring nodes is

$$\int dx(s - \sigma_r)E_S \tag{12}$$

in the present notation where dxE_S is the kinetic energy in a shell of thickness dx. Since σ_r is negligible by assumption in this section and s is constant for a given mode, kinetic energy itself becomes a conserved quantity. The mark on Figure 3 is drawn at the midpoint of the vertical range. It applies to the ultimate modes ($x_0 \to 0$), which, as the curve shows, have half their kinetic energy on the inner 11% of the solar radius. The lowest angular harmonics, $l \leq 3$, with $n > 2$ also have small lower boundaries $x_0 \leq 0.035$, which means that half their kinetic energy will concentrate on no more than the inner 15% of a radius. Since concentration means shorter radial wavelengths and larger relative velocities, the strongest shear fields will be near the origin and could be significant in mixing these solar layers.

Integer values of $\chi + \beta$ (evaluated at the top of the cavity) approximately correspond to n, the radial harmonic number, with $n = 0$ being the harmonic with no nodes in the cavity. This leads to the asymptotic expression, $n = 4.65(-s\lambda_1)^{0.5} + \beta$, based on the largest value on Figure 3 as all cavity boundaries closely approach the same two points—the center of the star and the base of the convection zone. The eigenvalue is approximately

$$s = \frac{-1}{\lambda_1}\left(\frac{n + 1/2}{4.65}\right)^2 . \tag{13}$$

A further simplification comes if the angular harmonic is also large. Then

$$\lambda_1 = 0.5l^3 , \qquad |m| = l \gg 1 , \tag{14a}$$

$$\lambda_1 = \frac{l^4}{2(l^2 - m^2)} , \quad |m| \neq l \gg 1 . \tag{14b}$$

Note that these expressions for large n and/or l depend on solar structure only through one constant, 4.65, which is the integral of $(\lambda_b x^{-2})^{0.5}$ over the entire nonconvecting shell divided by π. That integral is also prominent in an asymptotic formula (PBR) for large l, finite m, and any σ_r.

4. FULL SOLUTIONS

4.1. *Eigenvalues and Radial Dependence*

The r-mode equation (8) has the ideal form for visualizing solutions but requires knowing the second derivative of the buoyancy frequency, which is often very noisy when computed from a solar model. A less compact form (eq. [11] of PBR or eq. [3] of WB) involves only the first derivative of λ_b and was used here for numerical integrations. Each of these papers has a different misprint: in PBR use $g = -p'/\rho$, and in WB use $A = -g^{-1}\lambda_b$ with λ_b as defined here in equation (10). After applying two boundary conditions, the eigenvalues s and f_3 for a particular state (l, m, n) can be found. The simplest central boundary condition is $f_3 \propto x^l$. But the next higher approximation,

$$f_3 = \text{constant } x^l(1 + Kx^2) , \tag{15}$$

was used here because the integration did not start at the origin. The constant $K = s\lambda_1\lambda_b x^{-2}[(l + 2)(l + 3) - l(l + 1)]^{-1}$ must be evaluated at the first point of the integration, which was $x = 0.007$ in this work. In the Guenther et al. (1992) solar interior model used here, $\lambda_b x^{-2}$ approaches a constant, 8190, near the origin. Equation (15) was derived by writing f_3 and solar structure parameters as power series about the origin and substituting in the r-mode equation. Beyond the upper boundary of the resonant cavity, the amplitude must decline exponentially. Rising solutions can be rejected by adjusting s until a proper solution is found. All integrations were extended beyond the cavity and satisfy an upper boundary condition, $f_3 = 0$ at $x = 0.9$, which gives solutions valid within the cavity and sufficiently accurate in s.

Table 2 lists eigenvalues for 40 of the solutions computed, multiplied by 100 for easier reading. All the lowest harmonic states are shown, plus a few higher harmonics. When s is multiplied by $\varepsilon^2 \simeq 1.6 \times 10^{-5}$ it is apparent how very little

TABLE 2

EIGENVALUES (100s) FOR VARIOUS HARMONIC r-MODES

		n			
l	$\lvert m\rvert$	0	1	2	5
1.....	1	+0.33	−1.78	−4.66	−18.50
2.....	1	−9.97	−19.34	−31.11	−87.50
2.....	2	+3.42	+0.92	−0.22	−6.60
3.....	1	−9.69	−14.32	−20.79	−39.20
3.....	2	−4.97	−7.81	−12.21	−32.29
3.....	3	+6.72	+3.25	+1.64	−1.58
5.....	1	−9.05	−10.61	−13.85	−27.15
5.....	5	+12.41	+7.28	+4.92	+2.24
9.....	1	−7.26	−9.51	−10.24	−15.59
9.....	9	+19.33	+13.82	+10.57	+5.88

the complete oscillation frequency (eq. [3]) will depart from the pure toroidal value. This satisfies the condition for equation (4b) to be true; spheroidal motion is indeed negligible.

Eight radial eigenfunctions f_3 are plotted on Figure 4, normalized to unity at the first maximum. They illustrate the degree to which the harmonic numbers affect proximity to the two regions most likely to contain an excitation mechanism: the nuclear burning core and the upper layers where convective overshoot occurs. Figure 4*a* shows a low angular harmonic $(l, m) = (2, 2)$. The radial states are $n = 2$ and $n = 9$, for which $s = -0.00221$ and -0.2072, respectively. A separate computation of the mode's energy showed that, for the case $n = 9$, more than half the mode's energy is below the middle node at $x = 0.127$, and its half-energy point is at $x = 0.105$, which agrees with the asymptotic estimate in § 3. Even the $n = 2$ case shows this concentration toward the origin. Only the $n = 0$ and $n = 1$ modes were found to have noticeably less central concentration than the asymptotic value. Figure 4*b* shows the degree to which higher angular harmonics avoid the origin due to their initial x^l dependence. If one seeks some mechanism in the solar core to excite *r*-modes, then among the modes calculated here, those most favored would seem to be those of low l and, for a given l, those of smaller $|m|$. Trends on Figures 4*a* and 4*b* are also apparent in the PBR study of a convectively stable polytrope, which necessarily lacks the Sun's envelope and the correct decline of buoyancy frequency near the origin.

Figure 4*c* shows the only type of mode whose radial distribution might be favorable for excitation by convective overshoot. These are the lowest radial harmonic ($n = 0$) of each state where $|m| = l > 1$. They are free from the restraints of the asymptotic curve in Figure 3 because their long radial wavelengths throughout the cavity do not come close to satisfying the approximations made in § 3. These $n = 0$ modes are unique in approaching the upper boundary of the cavity except possibly for modes not calculated here with exceedingly large l. Already by $n = 1$, some concentration toward the origin is clear (Fig. 4*b*).

4.2. *Compressible Fraction (div/curl)*

It is sometimes useful to know how much of an oscillation is compressible ($\nabla \cdot \boldsymbol{\xi} \neq 0$) and how much is not ($\nabla \times \boldsymbol{\xi} \neq 0$). Wolff (1979) derived a "curl-divergence frequency" for *p*-modes and *g*-modes which showed where in a star the motion was curl-dominated and where it was mostly divergent. Compressible effects decreased for deeper locations in the Sun or lower oscillation frequencies. The same trend will be found below for *r*-modes, but the compressible portion will be much smaller everywhere and the analytic formula more complex.

The amplitudes, A_d and A_c, of divergence and curl motion will be defined by integrals over a complete spherical surface:

$$A_d^2 = \oint dS\,|\nabla \cdot \boldsymbol{\xi}|^2 \tag{16}$$

and

$$A_c^2 = \oint dS\,|\nabla \times \boldsymbol{\xi}|^2 \,. \tag{17}$$

Assuming that radiation pressure and time-dependent heat generation are negligible, the divergence equals $-(\gamma p)^{-1}\delta p$, where an expression for the Lagrangian pressure pertur-

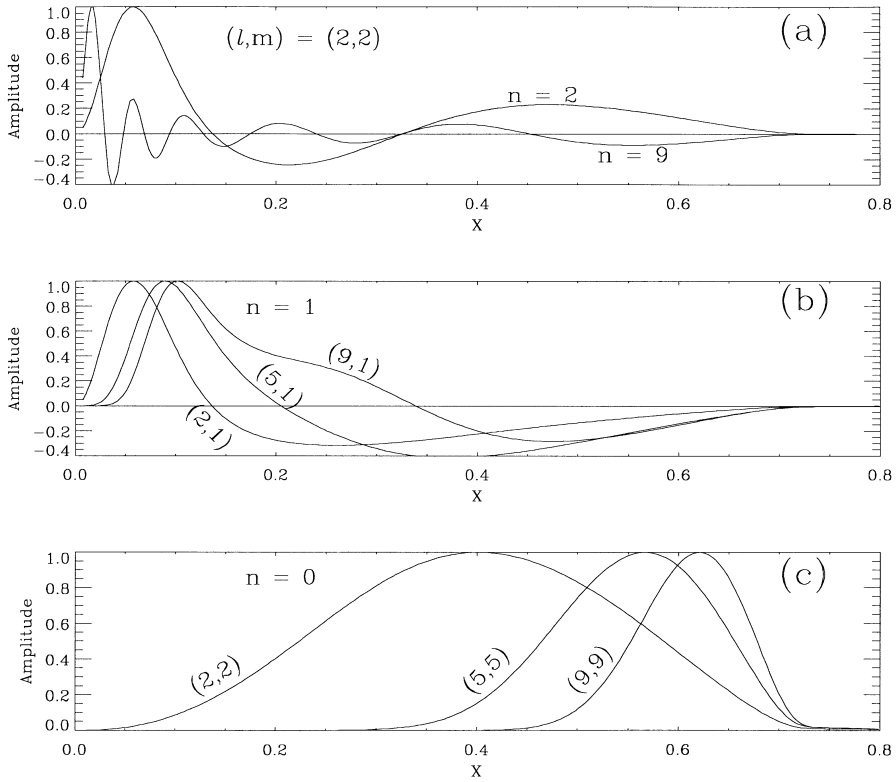


FIG. 4.—Radial eigenfunctions of *r*-modes are shown. The first two panels show the effect on proximity to the origin of (*a*) radial harmonic number n and (*b*) angular harmonic number l. Panel (*c*) shows the only modes found ($n = 0, |m| = l$), the activity of which is concentrated outward toward the base of the convection zone.

bation δp is available in PBR. It contains two associated Legendre polynomials $P^m_{l\pm1}$ which can be integrated exactly when inserted in equation (16). The curl also integrates exactly using $\varepsilon^2 \ll 1$ and equation (4b). The resulting ratio becomes

$$\frac{A_d}{A_c} = \frac{2i\varepsilon^2\sigma_0}{\gamma[l(l+1)]^{3/2}}\left(\frac{b_1}{b_2}\right)\frac{x}{H_p\lambda_b}, \tag{18}$$

The factor ε^2 makes the entire expression very small, $\sigma_0 = 2m[l(l+1)]^{-1}$, the square root of minus 1 means that the divergence is 90° out of phase with the curl, the b_i are defined shortly, and the last fraction containing the pressure scale height $H_p = -p/p'$ is plotted on Figure 5. It shows how strongly the compressible component is reduced relative to the incompressible part as one moves toward the center of the Sun. Between $x = 0.6$ and $x = 0.1$ their ratio becomes smaller by a factor of 28. In the vicinity of 0.6, equation (18) requires that the r-mode velocity compressing the fluid will be $\sim 10^{-6\pm1}$ of the toroidal velocity for any low harmonic mode. This differs strongly from r-modes trapped in the convective envelope the compressible components of which WB found to be $\sim$1000 times larger. Finally, A_d cannot remain small approaching the convection zone boundary, since λ_b is zero there. But this is a very thin region because A_d does not exceed $10^{-2}A_c$ until just a few kilometers before reaching the boundary.

The curl-divergence frequency is defined from equation (18) as $\sigma_{cd} = \sigma_0 A_c/A_d$. For direct comparison with the result (Wolff 1979) for p- and g-modes, convert from our dimensionless unit and divide by 2π to express, in hertz, the curl-divergence frequency of r-modes trapped below the convection zone:

$$\nu_{cd} = \frac{\varepsilon\Omega_g}{2\pi}\,\sigma_{cd}\,. \tag{19}$$

The quantity plotted in Figure 5 gives the overall trend of A_d/A_c. Smaller scale fluctuations occur due to the b_i which contain the radial eigenfunction f_3. This eigenfunction is the same as those in the literature, called C or $C_{lm}(x)$, except for a normalization constant that cancels from equation (18). In terms of constants (λ_2, D_l, and $K_l^{\pm}$) defined by PBR,

$$b_1^2 = kf_3^2 + \frac{\lambda_2}{D_l}\,xf_3\,f'_3 + \frac{1}{D_l}\,(xf'_3)^2\,,$$

and

$$b_2^2 = [1 + l(l+1)]f_3^2 + 2xf_3\,f'_3 + (xf'_3)^2\,,$$

where

$$k = l^6K_l^-\,K_{l+1}^+ + (l+1)^6K_{l-1}^-\,K_l^+\,.$$

This simplifies greatly if $l \gg 1$ and either f_3 or its derivative is negligible (high or low n). Then

$$\frac{A_d}{A_c} \simeq i\varepsilon^2\,\frac{1.7m}{l^3}\left(1 - \frac{m^2}{l^2}\right)^{1/2}\left(\frac{x}{H_p\lambda_b}\right), \qquad m^2 \neq l^2,\ \ f_3 \text{ or } f'_3 \text{ negligible}\,. \tag{20}$$

For these high harmonics, the compressible fraction at $x = 0.6$ is less than $3 \times 10^{-5}ml^{-3}$ and at $x = 0.1$ it is less than $1 \times 10^{-6}ml^{-3}$.

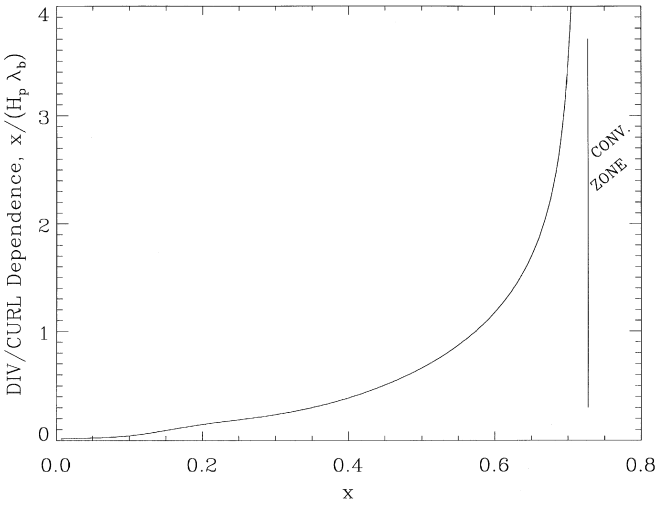


FIG. 5.—Overall trend of the divergence-curl ratio. It is also the ratio of compressible to incompressible components of solar r-mode motion when multiplied by the very small constant and fluctuations included in eq. (18).

5. MODE EXCITATION BY AN IMPOSED FORCE

5.1. *The Diagonal Coriolis Approximation*

Abandon dimensionless units and let all symbols hereafter carry their usual physical units. Assume that the nonconvecting solar interior rotates at a slow uniform rate Ω and that a time-dependent force/mass, $\boldsymbol{F}_m$, acts upon it. These solar layers represent a resonant cavity for g-modes and r-modes. In coordinates rotating at Ω, the momentum equation for a mode of small amplitude with displacement $\boldsymbol{\Psi}$ is

$$\frac{\partial^2\boldsymbol{\Psi}}{\partial t^2} + 2\boldsymbol{\Omega}\times\frac{\partial\boldsymbol{\Psi}}{\partial t} + \boldsymbol{L}(\boldsymbol{\Psi}) = \boldsymbol{F}_m(\boldsymbol{r}, t)\,, \tag{21}$$

where the oscillating forces due to pressure gradient, buoyancy, and self-gravitation are given by $\boldsymbol{L}(\boldsymbol{\Psi}) = [\nabla p + \rho\nabla W_0 + \rho_0\nabla W]\rho_0^{-1}$, which will cancel from the derivation below. Zero subscripts identify the equilibrium state, and $\boldsymbol{L}$ is made an explicit linear function of $\boldsymbol{\Psi}$ by using the mass and energy equations to eliminate p, ρ, and W (Cox 1980, chap. 15; Lynden-Bell & Ostriker 1967).

Follow the approach of Goldreich & Keeley (1977), whose equation (36) for a nonrotating case is the same as our equation (24) with $\boldsymbol{\Omega} = 0$. The well-known p-, g-, and r-modes solve the homogeneous equation ($\boldsymbol{F}_m = 0$)

$$-\sigma_j^2\,\boldsymbol{\xi}_j + 2i\sigma_j\boldsymbol{\Omega}\times\boldsymbol{\xi}_j + \boldsymbol{L}(\boldsymbol{\xi}_j) = 0\,, \tag{22}$$

where $\boldsymbol{\xi}_j(\boldsymbol{r})e^{i\sigma_j t}$ is the jth solution. Assume normalization and mutual orthogonality such that $\int dm\boldsymbol{\xi}_k^*\cdot\boldsymbol{\xi}_j = \delta_{kj}$, where dm is the mass element. Use the homogeneous solutions to solve equation (21) by expanding

$$\boldsymbol{\Psi} = \sum_j A_j\,\boldsymbol{\xi}_j\,e^{i\sigma_j t} \tag{23}$$

and determining the time-dependent functions A_j. Substituting this sum into equation (21), canceling $\boldsymbol{L}$ using equation (22), and operating with $\int dm\boldsymbol{\xi}_k^*\cdot$ gives

$$(\ddot{A}_k + 2i\sigma_k\dot{A}_k)e^{i\sigma_k t} + \sum_j i\Omega_{\mathrm{Cor}}\,\dot{A}_j\,e^{i\sigma_j t} = \int dm\boldsymbol{\xi}_k^*\cdot\boldsymbol{F}_m\,, \tag{24}$$

where $i\Omega_{\rm Cor} = 2\int dm\boldsymbol{\xi}_k^* \cdot \boldsymbol{\Omega} \times \boldsymbol{\xi}_j$ comes from the Coriolis force. There are only three nonzero terms in $\Omega_{\rm Cor}$: one for $j = k$ and two others in which j stands for $(l_k \pm 1, m_k)$. The diagonal term is easily derived using equation (4a) and properties of spherical harmonics:

$$\Omega_{\rm Cor}(j = k) = -2\Omega m_k \int dr\, r^2 \rho_0 \times (|f_3|^2 + |f_2|^2 + f_1\, f_2^* + f_1^*\, f_2)\,. \quad (25)$$

According to equation (4b) this is $\sim f_3^2$ when compared to the nondiagonal terms, which are $\sim f_3\, f_2$ and $\sim f_3\, f_1$. Therefore, only the diagonal term is needed in equation (24) unless the amplitude of mode k is so much weaker than its "neighbor" that $A(l_k, m_k) \sim \varepsilon^2 A(l_k \pm 1, m_k)$. Such weakly excited modes will be of little interest. Using equation (25) the first integral of equation (24) is

$$\dot{A}_k + i(2\sigma_k + \Omega_{\rm Cor})A_k = \int dt e^{-i\sigma_k t} \int dm\boldsymbol{\xi}_k^* \cdot \boldsymbol{F}_m\,. \quad (26)$$

Assume a critically damped force such that $\boldsymbol{F}_m = e^{-\gamma t}\boldsymbol{E}(r)$, and define its effective lifetime, $\tau = \gamma^{-1}$. (Do not confuse γ with the ratio of specific heats used earlier). Texts on mechanical resonance treat more general time dependences. Boundary conditions at $t = 0$ and ∞ are, respectively, $A_k = 0$ and a constant. The solution is

$$A_k = \frac{-I_k(1 - e^{-i\beta t})}{\gamma^2 + \sigma_k^2 + \beta\Omega_{\rm Cor}}\,, \quad (27)$$

where $\beta = \sigma_k - i\gamma$ and the integral $I_k = \int dm\boldsymbol{\xi}_k^* \cdot \boldsymbol{E}$ is performed over the volume within the cavity where $\boldsymbol{F}_m$ is nonzero.

5.2. *Convective Overshoot Driving Low Harmonic Modes*

Apply the above by letting F_m stand for overshoot at the base of the convective envelope—either the small-scale plumes ($\tau \sim 1$ day) or broad depressions caused by possible giant cells ($\tau \sim 100$ days). Uncertainty about penetration depths and τ values limits the results of this section to orders of magnitude. Only low harmonic oscillation modes are discussed so that their wavelengths exceed the corresponding dimension of the overshoot. Large horizontal sales are particularly interesting because they could most easily cause detectable modulation of features on the surface.

The small-scale overshoot is often studied (e.g., Roxburgh 1997; Zahn 1998; Freytag, Ludwig, & Steffen 1996). Numerical simulations show descending fluid contracting into narrow plumes (Rast 1997; Brummell, Hurlburt, & Toomre 1998). A plume reaching the base of the convection zone can have enough kinetic energy to penetrate about 1 pressure scale height into the stable layers (Singh, Roxburgh, & Chan 1995). But a smaller penetration depth, $\Delta < 0.1H_p$, is predicted by the mixing-length formalism and by more complete analytic theories (Canuto 1997). An estimate independent of convection theory shows $\Delta < 0.05H_p$ (Basu 1997) but this helioseismic measurement is a global average. Fritts, Vadas, & Andreassen (1998) use two representative values for effective lifetime: 8 days and 10–30 hr. For simplicity, let $\tau = 2$ days and $\Delta = 0.1H_p = 5.6$ Mm.

Giant convection cells have been detected—then, not detected—many times since the 1960s. Their velocities at the solar surface are near the noise level. Beck et al. (1998) cite some of this work and report what looks to me like a fairly solid detection. They see cells that extend over 40° of longitude and 10° of latitude. Velocity in the cell falls to $1/e$ of its initial value in 126 days. Cells of such size and lifetime must originate near the bottom of the convection zone where overturning times are months. The descending arm of the cell will push fluid below the base of the convection zone over a broad area by an unknown amount which is probably less than that for small-scale overshoots. Adopt for giant cells $\tau = 126$ days and $\Delta \sim 1$ Mm.

The critically damped $\boldsymbol{F}_m$ implies a radial penetration distance $(1 - e^{-\gamma t})\Delta$. Its second time derivative should match the radial component of $\boldsymbol{F}_m$, since $\boldsymbol{F}_m$ is an acceleration. This occurs if

$$\boldsymbol{E} = (-\hat{\boldsymbol{r}}\gamma^2\Delta + \hat{\boldsymbol{\phi}}c_1)h\,, \quad (28)$$

where $h = 1$ in the volume directly affected by the overshoot and zero elsewhere. The azimuthal component arises from solar rotation because the initial rotation speed of the overshoot is faster by $V = \Omega D \sin\vartheta$ than the ambient fluid, where it will come to rest. This is a mixing-length approach, and D is the radial distance between the final location of the overshooting mass and the place, earlier, where it rotated at the ambient speed of the convection zone. Fit the average deceleration, V/τ, to the time average of $\hat{\boldsymbol{\phi}} \cdot \boldsymbol{F}_m$ during τ by setting $c_1 = 1.6\gamma V$. The center of gravity of a giant cell is high above the base of the convection zone by about 1 density scale height (80 Mm), where conformance with the ambient rotation will be assumed. Thus, $D = 80$ Mm for a giant cell. For the small-scale events, which have a much smaller ratio of inertia to drag surface area, $D = \Delta$ seems a more reasonable choice.

With these parameters, we can compute an actual size for the eigenfunctions plotted in Figure 4*c* at the place $x = x_{\rm max}$ where each reaches its peak. Of the 5–10 giant cells at a typical time, just one acting alone drives the component $e^{i\sigma_k t}$ in equation (23) to a peak displacement of

$$\xi_k(x_{\rm max})A_k(t = \tau) \sim (2\text{ km}) \sin\vartheta(\Delta, \text{ in Mm}) \quad (29)$$

for the (5, 5, 0) mode. The displacement is twice as large for the (9, 9, 0) mode and smaller by a factor of 10 for (2, 2, 0). They could all be much more than kilometer size if energy accumulates over the years from other giant cells acting roughly in phase with the r-mode. Some degree of synchronization is expected because a giant cell loses less energy to turbulence if its descending portion enters ambient fluid which the r-mode is already pushing in the direction of the rotation velocity. Such a cell can grow stronger than an equivalent cell of opposite phase. Thus the presence of an r-mode favors the growth of those giant cells best located to pump energy into the r-mode. How many cycles this can go on before reaching equilibrium with loss mechanisms is unknown. In fact, the extreme sensitivity of large-scale convection to subtle changes near the base of a cell will make the strength of this interaction with r-modes very hard to evaluate definitively.

Small-scale overshoots are so numerous and short-lived that the tendency to synchronize with the r-mode is overwhelmed by their frequent need to overturn. Fritts et al. (1998) assume 10 Mm spacing which implies that there are $N = 30{,}000$ overshoots at a given time. Since synchronization is not important in this case, no accumulation over time is expected and the peak displacement of the excited r-mode is $\sim \xi_k A_k N^{1/2}$. In spite of the large N, this works

out to be less than 1% of the peak displacement caused by the one giant cell just discussed.

6. SUMMARY

Of the *r*-modes in the family trapped below the convective envelope, many concentrate their activity in the core, especially those with high n and low l. Most modes have at least half their kinetic energy less than 0.15 $R_\odot$ from the Sun's center and the highest-n modes approach the limit, 0.11 $R_\odot$. If such modes are excited in the Sun, the driving mechanism will almost certainly be in the core. The central concentration means shorter radial wavelengths, which would imply stronger shear fields and mixing.

A small subset of *r*-modes avoid the central regions and have their maximum amplitude closer to the base of the convection zone. These are the lowest radial harmonic of angular states in which $|m| = l$. For $2 \leq l \leq 9$ the maximum displacement amplitude is between 0.40 and 0.62 $R_\odot$. Mode excitation under the impact of an applied force was derived using an approximate Coriolis term appropriate for deep solar *r*-modes. The force from one so-called giant cell (Beck et al. 1998), can excite these *r*-modes to kilometer-sized displacements. Much larger displacement amplitudes could accumulate in the *r*-modes over time if they significantly assist the growth of the giant cells.

Oscillation frequencies of *r*-modes are remarkably close to the purely toroidal value in equation (1). Very small fractional deviations, $\varepsilon^2 s \sim 10^{-7}$ to 10^{-5}, were found for the modes computed here (Table 2). These deviations are roughly 1000 times smaller than WB found for *r*-modes trapped in the convective envelope.

Although the toroidal component of the motion is overwhelmingly dominant for linear *r*-modes, only the spheroidal component (nonzero f_1 and f_2 in eq. [4]) compresses the fluid. The ratio of compressible to incompressible displacement amplitudes, $A_d/A_c \sim 10^{-6}$ for low l modes, and Figure 5 shows its variation with radius.

This paper applies to small-amplitude oscillations in what has been called for several decades a "standard solar model." One excitation mechanism was explored in § 5. Other excitation and damping effects need consideration as well as coupling between the modes.

I thank D. B. Guenther for kindly supplying me with a detailed tabulation of the solar model of Guenther et al. (1992).

REFERENCES

Aizenman, M. L., & Smeyers, P. 1977, Ap&SS, 48, 123
Basu, S. 1997, MNRAS, 288, 572
Beck, J. G., Duvall, T. L., Jr., & Scherrer, P. H. 1998, Nature, 394, 653
Brummell, N. H., Hurlburt, N. E., & Toomre, J. 1998, ApJ, 493, 955
Canuto, V. M. 1997, ApJ, 489, L71
Chandrasekhar, S. 1933, MNRAS, 93, 390
———. 1961, Hydrodynamic and Hydromagnetic Stability (Oxford: Clarendon)
Cox, J. P. 1980, Theory of Stellar Pulsation (Princeton: Princeton Univ. Press)
Freytag, B., Ludwig, H.-G., & Steffen, M. 1996, A&A, 313, 497
Fritts, D. C., Vadas, S. L., & Andreassen, O. 1998, A&A, 333, 343
Goldreich, P., & Keeley, D. A. 1977, ApJ, 212, 243
Guenther, D. B., Demarque, P., Kim, Y.-C., & Pinsonneault, M. H. 1992, ApJ, 387, 372
Lockitch, K. H., & Friedman, J. L. 1999, ApJ, 521, 764
Longuet-Higgins, N. S. 1964, Proc. R. Soc. London A, 279, 446
Lynden-Bell, D., & Ostriker, J. P. 1967, MNRAS, 136, 293
Papaloizou, J., & Pringle, J. E. 1978, MNRAS, 182, 423
Provost, J., Berthomieu, G., & Rocca, A. 1981, A&A, 94, 126 (PBR)
Rast, M. P. 1997, SCORe '96: Solar Convection and Oscillations and Their Relationship, ed. F. P. Pijpers, J. Christensen-Dalsgaard, & C. S. Rosenthal (Dordrecht: Kluwer), 135
Roxburgh, I. W. 1997, SCORe '96: Solar Convection and Oscillations and Their Relationship, ed. F. P. Pijpers, J. Christensen-Dalsgaard, & C. S. Rosenthal (Dordrecht: Kluwer), 23
Saio, H. 1982, ApJ, 256, 717
Singh, H. P., Roxburgh, I. W., & Chan, K. L. 1995, ApJ, 295, 703
Smeyers, P. 1980, Space Sci. Rev., 27, 653
Smeyers, P., Craeynest, D., & Martens, L. 1981, Ap&SS, 78, 483
Tassoul, J.-L. 1978, Theory of Rotating Stars (Princeton: Princeton Univ. Press)
Thompson, M. J., et al. 1996, Science, 272, 1300
Unno, W., Osaki, Y., Ando, H., Saio, H., & Shibahashi, H. 1989, Nonradial Oscillations of Stars (Tokyo: Univ. Tokyo Press)
Wolff, C. L. 1979, ApJ, 227, 943
———. 1993, ApJ, 414, 892
———. 1998, ApJ, 502, 961
Wolff, C. L., & Blizard, J. B. 1986, Sol. Phys., 105, 1 (WB)
Zahn, J.-P. 1998, Space Sci. Rev., 85, 79